

000 001 002 003 004 005 006 007 008 009 010 011 012 013 014 015 016 017 018 019 020 021 022 023 024 025 026 027 028 029 030 031 032 033 034 035 036 037 038 039 040 041 042 043 044 045 046 047 048 049 050 051 052 053 HALLUCINATION-AWARE INTERMEDIATE REPRESENTATION EDIT IN LARGE VISION-LANGUAGE MODELS CONFERENCE SUBMISSIONS

Anonymous authors

Paper under double-blind review

ABSTRACT

Large Vision-Language Models have demonstrated exceptional performance in multimodal reasoning and complex scene understanding. However, these models still face significant hallucination issues, where outputs contradict visual facts. Recent research on hallucination mitigation has focused on retraining methods and Contrastive Decoding (CD) methods. While both methods perform well, retraining methods require substantial training resources, and CD methods introduce dual inference overhead. These factors hinder their practical applicability. To address the above issue, we propose a framework for dynamically detecting hallucination representations and performing hallucination-eliminating edits on these representations. With minimal additional computational cost, we achieve state-of-the-art performance on existing benchmarks. Extensive experiments demonstrate the effectiveness of our approach, highlighting its efficient and robust hallucination elimination capability and its powerful controllability over hallucinations. Our code will be released.

1 INTRODUCTION

Large Vision-Language Models (LVLMs) (Bai et al., 2023b; Dai et al., 2023; Liu et al., 2024b; Zhu et al., 2023) have made remarkable advancements in recent years, demonstrating the ability to generate context-aware language outputs based on visual understanding. By integrating visual information into Large Language Models (LLMs), LVLMs have demonstrated strong capabilities in tasks such as multimodal reasoning (Lu et al., 2022) and complex scene understanding (Luo et al., 2024). However, LVLMs currently face the issue of hallucination, where the generated responses contradict the actual visual content.

Recently, many approaches (Leng et al., 2024; Liu et al., 2024a; Yin et al., 2024b; Zhao et al., 2023) have been proposed to mitigate hallucinations in LVLMs, which can be broadly categorized into retraining methods and Contrastive Decoding (CD) methods. As illustrated in Fig. 1 (a), retraining methods aim to alleviate hallucinations by constructing specialized datasets that target hallucination phenomena and introducing new training paradigms (Jiang et al., 2024a; Fu et al., 2024; Lu et al., 2023). In contrast, Fig. 1 (b) illustrates the paradigm of CD methods, which mitigate hallucination during inference. The method can work by contrasting the output token probabilities of the original response with those of a weakened variant that is more susceptible to hallucination. CD methods effectively reduce hallucinations without requiring retraining or additional data (Leng et al., 2024; Huo et al., 2024; Manevich & Tsarfaty, 2024).

Although both methods have shown promising results in hallucination mitigation, they still face some notable limitations: 1) Retraining methods require substantial data collection and computational resources for partial or full model fine-tuning. However, both the high cost of dataset construction and the heavy computational burden (*i.e.*, they need to retrain the LVLM) limit the practical applicability of these methods. 2) Contrastive decoding methods, while more efficient in design, introduce high computational overhead. They require two forward passes per inference—one for generating the original output and another for producing a deliberately weakened variant prone to hallucination—which significantly increases latency. Moreover, they uniformly adjust the probability of all tokens without distinguishing whether a token is actually prone to hallucination. For instance,

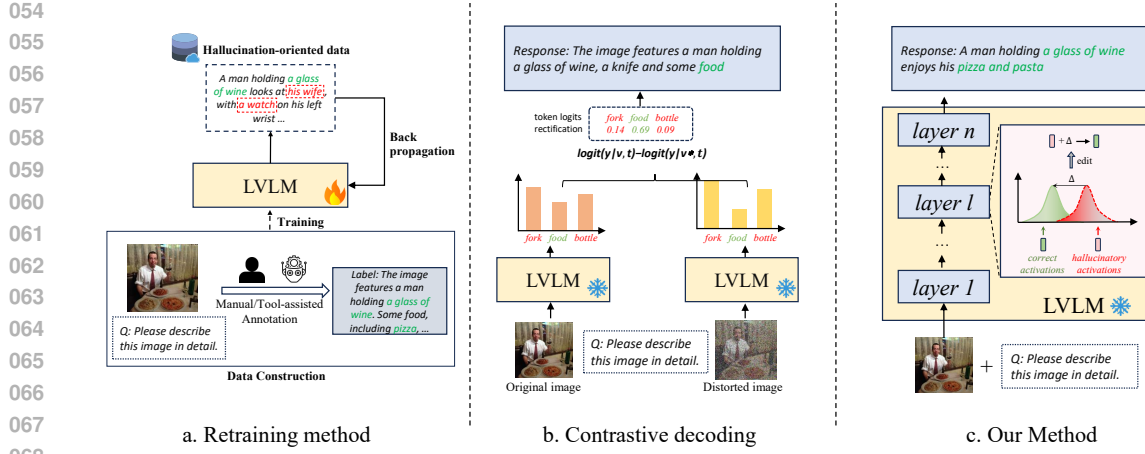


Figure 1: Comparison of mainstream hallucination mitigation paradigms. (a) Retraining-based methods: Constructing hallucination-specific datasets and training frameworks. (b) Contrastive decoding methods: Comparing the original probability distribution with a perturbed one. (c) Our method: Editing intermediate representations of LVLMs.

common tokens like “in,” “on,” or “from” rarely cause such issues. The one-size-fits-all adjustment leads to unnecessary computation and may harm output coherence. 3) Finally, hallucinations are not inherently harmful in tasks like creative writing (Jiang et al., 2024b), where appropriate hallucination can enhance expressiveness. However, most existing methods lack the ability to control the degree of hallucination, limiting their applicability in broader use cases where flexible generation is desired.

Recent studies on LLMs (Azaria & Mitchell, 2023; Chen et al., 2024b) have shown that a model’s internal representations encode cues about the truthfulness of statements, enabling hallucination detection without external knowledge. Building on these insights, recent research on LVLMs (Li et al., 2024; Duan et al., 2025) demonstrates that similar techniques can be applied to multimodal settings, where hallucination detection can be effectively performed through simple classifiers trained on intermediate features. This suggests that authentic and hallucinatory features in LVLMs are clearly separable in the latent space. This raises a natural question: *Can we leverage this inherent separation to effectively eliminate hallucinations?*

Based on the above discussion, we propose **HIRE** (Hallucination-aware Intermediate Representation Edit), a feature-editing framework that dynamically detects and mitigates hallucinations at the intermediate representation level. As shown in Fig. 1 (c), instead of costly retraining, we propose to mitigate hallucinations at the feature level without modifying the LVLM’s weights. Specifically, we first introduce a module, *Editor*, that learns to identify and isolate hallucination-related components by modeling both semantic invariance and hallucinatory differences between authentic and hallucinated responses, while preserving the underlying semantic information. Moreover, since uniformly editing all tokens leads to unnecessary computational overhead, we design a lightweight *Router* to selectively edit only tokens with high hallucination risk. Lastly, to enable more flexible hallucination control, we introduce a *Hallucination Regulator*, which allows dynamic control over hallucination levels via a simple hyperparameter. Overall, our main contributions are:

- 1) We introduce a new paradigm for hallucination mitigation, which reduces fabricated content by modifying intermediate representations without requiring retraining models or doubling inference costs.
- 2) We propose a new framework, HIRE, that dynamically detects and edits intermediate representations with high hallucination. Meanwhile, the proposed method can control the degree of hallucinations to adapt to different user requirements by adjusting the editing intensity.
- 3) We validate the effectiveness of the proposed method through extensive experiments and achieve state-of-the-art performance on three benchmarks.

108 **2 RELATED WORK**
109110 **2.1 LARGE VISION-LANGUAGE MODELS**
111112 Building on the success of Large Language Models (LLMs) (Bai et al., 2023a; Brown et al., 2020;
113 Chiang et al., 2023; Touvron et al., 2023) and cross-modal learning (Radford et al., 2021; Dosovitskiy et al., 2020), Large Vision-Language Models (LVLMs) achieve breakthrough performance by
114 integrating visual perception and language generation capabilities, excelling in tasks such as image
115 captioning (Hossain et al., 2019), visual question answering (Antol et al., 2015), and multimodal
116 reasoning (Lu et al., 2022). A typical LVLM architecture comprises three core components: a visual
117 encoder for hierarchically image feature extraction like CLIP (Radford et al., 2021); a cross-modal
118 alignment module implemented via linear projection layers or advanced architecture like Q-Former
119 (Li et al., 2023b); a large language model fine-tuned through instruction tuning for context-aware
120 text generation. Despite these advancements, LVLMs inherently suffer from hallucination, where the
121 generated text exhibits semantic inconsistencies with the input visual content.
122123 **2.2 MITIGATING HALLUCINATIONS IN LVLMs**
124125 Recently, multiple strategies have been proposed to address hallucination in LVLMs, which can be
126 broadly categorized into retraining methods and Contrastive Decoding (CD) methods. Retraining
127 methods retrain LVLMs using carefully constructed datasets and training paradigms specifically
128 designed to address hallucinations. HA-DPO (Zhao et al., 2023) fine-tunes LVLMs using style-
129 consistent hallucination sample pairs to promote non-hallucinatory outputs. HDPO (Fu et al., 2024)
130 further targets diverse causes of hallucinations by constructing specialized preference pairs for visual
131 distraction, long-context generation, and multimodal conflicts. In contrast, CD methods mitigate
132 hallucinations by comparing the output distributions from the original and perturbed inputs, without
133 requiring any model parameter updates. VCD (Leng et al., 2024) introduces noise into visual
134 inputs to amplify hallucinations and suppresses them by contrasting perturbed and original token
135 distributions. SID (Huo et al., 2024) retains only the least important visual tokens after shallow
136 processing to amplify vision-text association hallucinations. Unlike previous works, we propose to
137 mitigate hallucinations by detecting and editing hallucinated representations, avoiding the need for
138 heavy training resources and the cost of dual inference.
139140 **3 PRELIMINARY**141 LVLMs have garnered significant attention due to their capacity to combine visual and textual
142 information for generation tasks. These models take both an image and a textual prompt as input.
143 Given an image, it is firstly processed by a visual encoder and a cross-modal interface. Subsequently,
144 the visual information v and the text-based query q are combined and fed into the LLM for further
145 processing. The LLM p_θ is a parameterized model that maps the input to a probability distribution
146 over the next token. Generally, the LLM architecture typically consists of stacked Transformer layers
147 (Vaswani et al., 2017), each comprising multi-head self-attention and a feed-forward network (FFN).
148 After passing through all L layers, the final hidden states are projected into the vocabulary space to
149 produce a probability distribution y_t over the next token. The above process can be formulated as:
150

151
$$y_t \sim p_\theta(y_t | v, q, y_{<t}), \quad (1)$$

152

153 where y_t is the t -th generated token, and $y_{<t}$ represents the previous tokens. However, the generated
154 sentences often suffer from hallucinations, where the output contradicts the real visual input.
155156 **4 METHOD**
157158 Current methods primarily employ retraining methods (Fu et al., 2024; Zhao et al., 2023) or CD
159 methods (Leng et al., 2024; Wang et al., 2024) to mitigate hallucinations. However, retraining
160 methods suffer from training resource burdens, while CD methods incur dual computational cost
161 during inference. Moreover, these approaches are incapable of achieving controllable generation of
hallucinations. Motivated by the separability of hallucinated and truthful representations in the latent

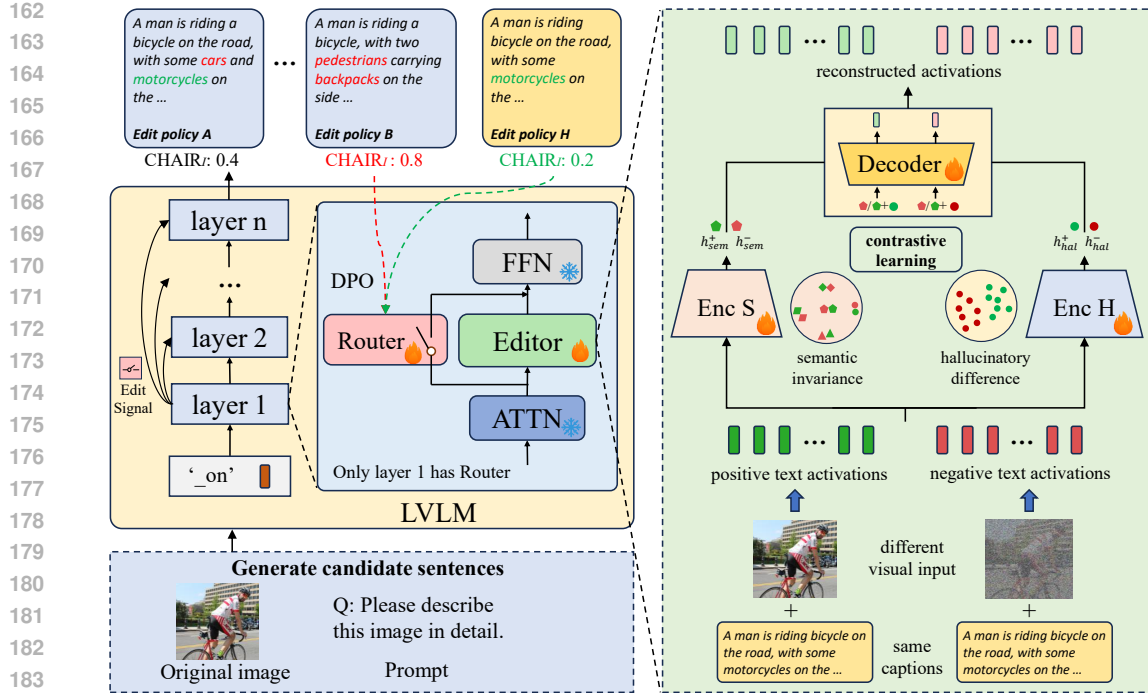


Figure 2: Overview of HIRE. Our framework consists of two key components: the Editor, which learns semantic invariance and hallucinatory difference through contrastive learning, and the Router, which learns efficient editing strategies through DPO.

space (Li et al., 2024; Duan et al., 2025), we propose a feature editing approach **HIRE**. As shown in Fig.2, HIRE dynamically identifies hallucination-prone components within representations and edits them by projecting features onto low-hallucination directions in the representation space.

To eliminate hallucination through editing and identify optimal editing strategies, we must address two key challenges: (1) how to determine the direction for obtaining hallucination-reduced representations, and (2) how to identify which token representations require editing. For the first challenge, we propose constructing hallucination-reduced representations by analyzing the divergence between high-hallucination and low-hallucination representations and then editing along this divergence direction. For the second challenge, our method autonomously learns effective editing strategies, enhancing the success rate of edits while minimizing ineffective changes. The following sections will detail our approach in terms of model architecture and optimization.

4.1 MODEL STRUCTURE

Editor. Based on the established correlation between hallucination phenomena and attention distributions (An et al., 2024; Huo et al., 2024), we identify the attention-layer representations at each transformer layer as our editing targets. The further analysis about the effect of editing different layers can be found in Appendix D.1. However, due to the entanglement between the representations of hallucinated and non-hallucinated texts (Jiang et al., 2024a), direct manipulation may disrupt semantic integrity (Li et al., 2023c; Chen et al., 2024c; Zhang et al., 2024). Inspired by (Zhang et al., 2024), we design a dual-encoder autoencoder G_ϕ that enables hallucination suppression while preserving semantics. Specifically, the G_ϕ consists of a semantic encoder E_{sem} , a hallucinatory encoder E_{hal} , a multi-head attention module f_{attn} , and a decoder D . Given the t -th token in attention-layer representations from l -th layer h_{tl} , the input representations are processed by both encoders to yield semantic representations $h_{tl,\text{sem}}$ and hallucinatory representations $h_{tl,\text{hal}}$, which can be formulated as:

$$h_{tl,\text{sem}} = E_{\text{sem}}(h_{tl}), \quad h_{tl,\text{hal}} = E_{\text{hal}}(h_{tl}). \quad (2)$$

216 To ensure correct editing, we compute the hallucination-reduction direction δ_l by averaging token-
 217 level differences between authentic and hallucinated representations within the hallucinatory subspace.
 218 The semantic and hallucinatory representations are fused and decoded to yield an optimized editing
 219 direction Δ_{tl} , which is the direction of targeted feature editing. The Δ_{tl} are obtained as follows:
 220

$$221 \quad \Delta_{tl} = D(h_{tl,sem} + f_{attn}(h_{tl,sem}, h_{tl,hal} + \delta_l)) - D(h_{tl,sem} + f_{attn}(h_{tl,sem}, h_{tl,hal} - \delta_l)), \quad (3)$$

223 where the f_{attn} denotes an attention fusion of $h_{tl,sem}$ (serving as query) and $h_{tl,hal}$ (serving as key and
 224 value). Overall, the δ_l aims to identify hallucination-reduced directions that are irrelevant to specific
 225 tokens within the hallucinatory subspace, while the Δ_{tl} leverages the δ_l to obtain token-specific
 226 hallucination-reduced directions in the original representation space.

227 **Router.** To avoid unnecessary editing operations on hallucination-free representations, we introduce
 228 a lightweight module, Router R_θ . Motivated by the observed layer redundancy in LVLMs, where
 229 deeper layers tend to exhibit high similarity (Wu et al., 2023; Suo et al., 2024), as well as by recent
 230 findings indicating that shallow layers preserve more informative representations (Wang et al., 2025;
 231 Chen et al., 2024a), we employ an MLP that takes the first-layer transformer representation h_{t0}
 232 as input and produces a binary decision c . This signal determines whether editing is required: if
 233 $c = 1$, the Editor is activated for all subsequent layers; otherwise, no editing is performed. Further
 234 experiments exploring alternative layer-wise decision strategies are provided in Appendix D.2]. With
 235 an editing strength α introduced, the editing process can be formulated as follows:

$$237 \quad h_{tl,aug} = \begin{cases} h_{tl} + \alpha \cdot \Delta_{tl} & \text{if } c = 1, \\ h_{tl} & \text{if } c = 0, \end{cases} \quad (4)$$

240 where $h_{tl,aug}$ denotes edited representations, and the $\alpha \in [-1, 1]$ controls the direction and intensity
 241 of editing. A positive α suppresses hallucination by steering features toward low-hallucination
 242 directions, while a negative α amplifies them, enabling flexible control over hallucination levels.
 243

244 4.2 MODEL OPTIMIZATION

246 The above computation reveals that the Editor G_ϕ and the Router R_θ are critical to detecting and
 247 correcting hallucination-related features. However, optimizing them is challenging due to the lack
 248 of labeled training data. Therefore, we introduce contrastive learning and DPO strategy to train the
 249 Editor G_ϕ and the Router R_θ , respectively. To disentangle hallucinatory patterns from semantic
 250 content, we use contrastive learning to optimize the Editor G_ϕ . Specifically, $H_{l,sem} = \{h_{tl,sem}\}_{t=1}^T$
 251 (T denotes the number of tokens) should have high similarity to semantically identical representations
 252 and low similarity to those with different meanings. Conversely, $H_{l,hal} = \{h_{tl,hal}\}_{t=1}^T$ exhibits high
 253 similarity within group similarity (hallucinated or authentic), but low cross-group similarity regardless
 254 of token semantics. To optimize the Router R_θ , we maximize the likelihood ratio between effective
 255 edits and ineffective ones by introducing DPO (Rafailov et al., 2023), which learns from pairwise
 256 data by increasing the likelihood of preferred responses while suppressing less desirable ones.

257 4.2.1 DATA CONSTRUCTION

259 Based on the finding that visual uncertainty amplifies hallucinations in LVLMs (Leng et al., 2024),
 260 we obtain authentic and hallucinated representations by pairing identical textual inputs with both
 261 intact and visually-degraded images. The positive sample uses the original image to produce more
 262 faithful outputs, while the negative sample uses a noised version of the image, weakening visual
 263 grounding and increasing hallucination. The resulting intermediate representations are denoted as
 264 $H_l^+ = \{h_{tl}^+\}_{t=1}^T$ and $H_l^- = \{h_{tl}^-\}_{t=1}^T$. Our framework is also compatible with other hallucination
 265 induction techniques; comparative experiments are provided in the Appendix D.3.

266 To obtain pairwise preference data, we generate N candidate captions for each image by applying
 267 different editing action sequences during greedy decoding, where each sentence S_n of length T_n
 268 has corresponding representations $\{h_{0t}\}_{t=1}^{T_n}$ and editing decision trajectory $\{c_t\}_{t=1}^{T_n}$. We quantify
 269 hallucination severity using the CHAIR_I metric (Rohrbach et al., 2018). The most and least faithful
 sentences are used to construct preference pairs (h^+, c^+) and (h^-, c^-) for the Router training.

270 4.3 TRAINING PROCESS
271

272 **Editor.** We apply contrastive learning to both the semantic and hallucinatory encoders. The semantic
273 encoder aims to preserve semantic information by maximizing the similarity between corresponding
274 tokens in positive and negative samples, while minimizing the similarity for non-matching tokens. In
275 contrast, the hallucinatory encoder focuses solely on hallucination-related signals and is trained to
276 separate positive and negative samples regardless of their semantic similarity. The loss formulations
277 are defined as follows, where negative samples are formulated similarly:

$$278 \quad \begin{aligned} 279 \quad L_{tl,sem}^+ &= \mathcal{L}_{\text{InfoNCE}}(h_{tl,sem}^+, h_{tl,sem}^-, H_{l,sem}^+), \\ 280 \quad L_{tl,hal}^+ &= \mathcal{L}_{\text{InfoNCE}}(h_{tl,hal}^+, H_{l,hal}^+, H_{l,hal}^-), \end{aligned} \quad (5)$$

282 where $\mathcal{L}_{\text{InfoNCE}}$ (Oord et al., 2018) encourages the anchor to be closer to positive samples than to
283 negatives, $h_{tl,sem}^\pm$ and $h_{tl,hal}^\pm$ denote the semantic and hallucinatory embeddings of token t at layer
284 l , and $H_{l,sem}^\pm$, $H_{l,hal}^\pm$ are the sets of token embeddings $h_{tl,sem}^\pm$ and $h_{tl,hal}^\pm$. The learned semantic and
285 hallucinatory representations are fused through a multi-head attention f_{attn} and decoded to predict the
286 original feature. To ensure both faithful reconstruction and effective editing, a reconstruction loss and
287 an editing loss can be formulated as follows, where negative samples are calculated similarly:

$$288 \quad \begin{aligned} 289 \quad L_{tl,recon}^+ &= \text{MSE}(h_{tl}^+, D(h_{tl,sem}^+ + f_{\text{attn}}(h_{tl,sem}^+, h_{tl,hal}^+))), \\ 290 \quad L_{tl,edit}^+ &= \text{MSE}(h_{tl}^+, D(h_{tl,sem}^- + f_{\text{attn}}(h_{tl,sem}^-, h_{tl,hal}^+))), \end{aligned} \quad (6)$$

292 where h_{tl}^\pm denote the original representations of the token t at layer l of positive and negative samples.
293 Averaging the sum of four loss terms across tokens and layers yields the final training objective \mathcal{L}_e .
294

295 **Router.** To guide the model towards optimal editing strategies, we adopt Direct Preference Optimiza-
296 tion (DPO) (Rafailov et al., 2023), which reformulates reward maximization as a policy likelihood
297 ranking problem. Unlike standard DPO that requires pairwise comparisons between a learnable
298 policy π_θ and a reference model π_{ref} , our implementation eliminates the reference model based on
299 recent findings (Meng et al., 2024) demonstrating its removability. The simplification is suitable for
300 training the Router from scratch rather than fine-tuning an existing policy. Given paired state-action
301 sequences (h^+, c^+) (preferred) and (h^-, c^-) (non-preferred), the optimization objective becomes:

$$302 \quad \mathcal{L}_r = -\mathbb{E}_{(h,c)} [\log \sigma (\beta (\log \pi_\theta(h^+, c^+) - \log \pi_\theta(h^-, c^-)))], \quad (7)$$

304 where \mathcal{L}_r denotes the Router’s training loss, π_θ represents the learnable policy (Router), $\sigma(\cdot)$ is the
305 sigmoid function, and $\beta = 0.1$ serves as a scaling factor regulating optimization intensity. Finally,
306 the total loss for optimizing both the Editor and the Router can be formulated as:

$$308 \quad \mathcal{L}_{\text{total}} = \mathcal{L}_e + \mathcal{L}_r. \quad (8)$$

310 5 EXPERIMENTS
311312 5.1 EXPERIMENTAL SETTINGS
313

314 **Dataset.** We evaluate our method on three benchmarks: CHAIR (Rohrbach et al., 2018), POPE (Li
315 et al., 2023d), and AMBER (Wang et al., 2023). CHAIR measures object hallucination in image
316 captions, calculating the proportion of objects mentioned in the text but missing from the ground-truth
317 annotations. It provides object-level (CHAIR) and sentence-level (CHAIRs) scores, with lower
318 values indicating fewer hallucinations. We evaluate on 500 images randomly sampled from the
319 MSCOCO (Lin et al., 2014) dataset. POPE assesses object hallucination in multimodal question
320 answering using three object-sampling strategies (random, popular, adversarial) and binary queries
321 like “Is there a <object> in the image?”. Evaluation is based on 9,000 question-answer pairs from
322 MSCOCO. AMBER evaluates hallucinations in LVLMs, using 1,004 generative instances and 14,216
323 discriminative instances annotated for existence, attribute, and relation hallucinations, providing a
324 comprehensive framework for hallucination identification and classification.

324
325
326 Table 1: Evaluation results on the CHAIR benchmark with LLaVA-1.5.
327
328
329

Method	LLaVA-1.5(Liu et al., 2024b)			InstructBLIP(Dai et al., 2023)		
	$\text{CHAIR}_S \downarrow \text{CHAIR}_I \downarrow \text{TFLOPs} \downarrow$					
baseline	51.3	16.8	10.23	51.0	24.2	2.77
Max new tokens set to 512						
OPERA(Huang et al., 2024)	45.2	12.7	-	47.4	12.9	-
SID(Huo et al., 2024)	44.2	12.2	-	42.3	12.4	-
ICD(Wang et al., 2024)	47.4	13.9	20.63	46.3	15.3	5.64
VCD(Leng et al., 2024)	46.8	13.2	20.46	44.0	13.6	5.61
M3ID(Favero et al., 2024)	48.3	13.5	20.71	45.2	13.9	5.70
AVISC(Huo et al., 2024)	45.2	13.4	20.08	43.9	13.5	5.63
Octopus(Suo et al., 2025)	39.2	11.1	21.39	40.6	12.1	5.87
Projectaway(Jiang et al.)	42.0	12.2	-	43.8	12.5	-
VTI(Liu et al., 2025)	35.8	11.1	-	43.4	11.8	-
Ours(HIRE)	30.2	9.7	11.81	39.0	11.5	3.45
Max new tokens set to 64						
baseline	20.4	6.2	8.91	25.4	8.2	1.89
M3ID+DPO(Favero et al., 2024)	13.5	5.7	-	-	-	-
Nullu(Yang et al., 2025)	17.0	5.9	-	-	-	-
Ours (HIRE)	15.2	5.4	9.18	14.8	5.4	2.32

340
341
342
343
344
345
346
347
348 **Implementation Details.** We train the Editor and the Router on the training split of the MSCOCO
349 dataset, using 2,000 randomly selected samples. The relationship between performance and data
350 size is shown in Appendix D.4. Training is performed for 10 epochs with a batch size of 1. For the
351 Editor, we use the AdamW (Loshchilov & Hutter) optimizer (learning rate 1×10^{-3}) and a Cosine
352 Annealing scheduler (a minimum learning rate of 1×10^{-5}). For the Router module, we set the
353 group size to 10 and use the Adam optimizer (Kingma & Ba, 2014) (learning rate 1×10^{-4}) and a
354 Cosine Annealing scheduler (a minimum learning rate of 1×10^{-6}). We report the results of our
355 method with a consistent edit strength α set to 1. All experiments were performed on four 3090
356 GPUs. Further discussions on the different training configuration are provided in the Appendix D.5.
357
358
359
360

5.2 RESULTS ON BENCHMARKS

361
362 We conduct experiments on LLaVA-1.5 (Liu et al., 2024b) and InstructBLIP (Dai et al., 2023) across
363 three widely used benchmarks: CHAIR (Rohrbach et al., 2018), POPE (Li et al., 2023d), and AMBER
364 (Wang et al., 2023), with related results from (Suo et al., 2025; Xing et al., 2024; Huo et al., 2024;
365 Jiang et al., 2024a; Liu et al., 2025; Jiang et al.). Overall, our method consistently outperforms existing
366 approaches while maintaining efficient inference. As shown in Table 1, it reduces sentence-level and
367 instance-level hallucinations by $\sim 40\%$ and $\sim 50\%$ respectively on both LLaVA-1.5 and InstructBLIP
368 in the long description scene (max new tokens set to 512). Additionally, in the short description
369 scene (max new tokens set to 64), our method also demonstrates reliable hallucination mitigation
370 capabilities. Table 2 shows that our method achieves improvements of 1.48/3.79 and 0.48/1.99 over
371 the state-of-the-art method Octopus(Suo et al., 2025) on the two models on the accuracy and F1
372 score, demonstrating superior performance in discriminative tasks. As shown in Table 3, our method
373 achieves the highest AMBER scores—an indicator that averages performance across generative and
374 discriminative tasks. Compared to the baseline, it significantly improves AMBER scores by 7.54
375 on LLaVA-1.5 and 6.38 on InstructBLIP. In addition, benefiting from the lightweight nature of our
376 editing strategy and the selective token editing enabled by the Router, our method introduces minimal
377 inference overhead. In summary, our approach effectively mitigates hallucination in both generative
378 and discriminative tasks, with only a small additional overhead. Additional analysis and results on
379 generalization and stability can be found in Appendix D.6 and Appendix D.7.

378
379
380
381 Table 2: Evaluation results on the POPE benchmark on the MS COCO datasets with LLaVA-1.5 and
382 InstructBLIP.
383
384

Method	Random		Popular		Adversarial		ALL		TFLOPs↓
	Acc.	F1	Acc.	F1	Acc.	F1	Acc.	F1	
LLaVA-1.5-7B	83.77	81.94	82.57	80.86	79.77	78.47	82.04	80.42	8.13
Referenced Results									
+HACL	88.59	88.70	87.84	87.36	86.54	85.73	87.66	87.26	-
+VTI	89.50	88.89	87.36	86.69	82.57	82.11	86.48	85.90	-
Comparable Results									
+ICD	87.51	83.28	83.15	83.91	79.13	80.41	83.26	82.53	-
+ConVis	84.70	-	83.20	-	81.10	-	83.00	-	-
+OPERA	84.40	-	83.40	-	81.20	-	83.00	-	-
+VCD	85.43	83.99	83.17	81.94	80.27	79.49	82.96	81.81	16.26
+M3ID	86.13	81.85	82.07	80.77	79.50	78.15	82.57	80.26	16.26
+AVISC	84.67	82.21	83.67	81.27	81.83	79.55	83.39	81.01	16.26
+Octopus	87.51	85.40	85.20	84.19	82.22	81.44	85.79	83.44	16.34
+Ours	90.37	90.25	87.70	87.86	83.73	83.56	87.27	87.23	10.62
InstructBLIP	81.53	81.19	78.47	78.75	77.43	78.00	79.14	79.31	1.08
+ICD	84.36	83.82	77.88	78.70	75.17	77.23	79.14	79.92	-
+OPERA	84.57	83.74	78.24	79.15	74.59	76.33	79.13	79.74	-
+VCD	82.03	81.56	79.13	79.20	77.23	77.72	79.46	79.49	2.16
+M3ID	82.33	81.53	80.90	80.42	78.53	78.49	80.59	80.15	2.16
+AVISC	86.03	84.41	84.27	82.77	81.83	80.67	84.04	82.62	2.16
+Octopus	86.63	85.30	84.90	83.55	82.83	81.43	84.79	83.43	2.27
+Ours	90.30	89.83	84.03	84.25	81.47	82.17	85.27	85.42	1.25

403
404 Table 3: Evaluation results on the AMBER benchmark with LLaVA-1.5 and InstructBLIP.
405

Model	Setting	Generative					Discriminative			AMBER↑
		CHAIR↓	Cover↑	Hal↓	Cog↓	TFLOPs↓	Acc.↑	F1↑	TFLOPs↓	
LLaVA-1.5	baseline	8.0	44.5	31.0	2.2	9.89	67.00	71.10	8.07	81.58
	VCD	6.7	46.5	27.8	2.0	19.55	67.30	71.10	16.14	82.20
	M3ID	6.0	48.9	26.0	1.5	19.81	67.25	70.90	16.14	82.25
	AVISC	6.3	46.6	25.6	2.0	19.45	70.70	75.45	16.14	84.60
	Octopus	4.8	49.2	23.4	1.2	20.48	76.70	82.70	16.35	88.95
	Ours	4.6	49.9	20.4	1.5	11.73	79.20	82.83	10.58	89.12
InstructBLIP	baseline	8.4	46.4	31.1	2.6	2.93	68.20	74.60	1.04	83.10
	VCD	7.6	47.7	29.9	2.2	6.11	69.65	75.90	2.08	84.15
	M3ID	6.9	47.2	27.5	2.2	5.87	69.05	75.25	2.08	84.20
	AVISC	6.7	46.7	28.0	2.6	6.09	72.60	78.60	2.08	85.95
	Octopus	6.1	48.5	22.2	1.3	6.47	74.00	79.70	2.19	86.80
	Ours	5.3	49.3	23.8	1.8	3.57	78.34	84.26	1.21	89.48

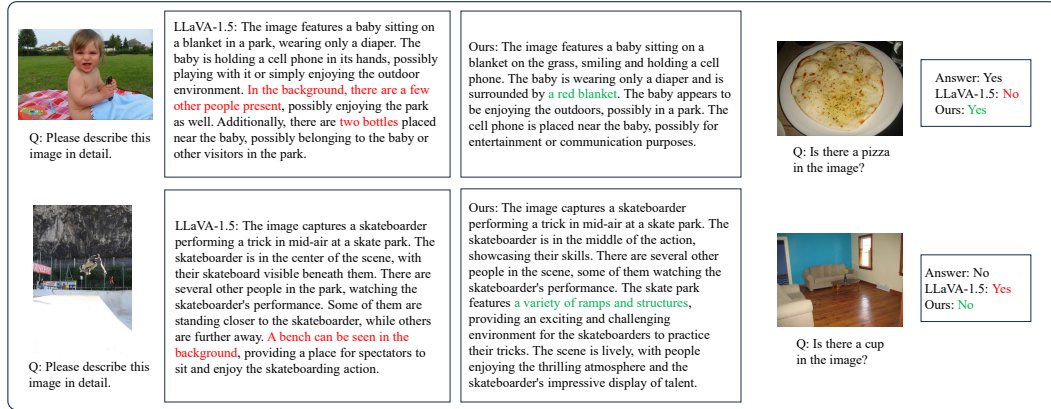
419
420
421 5.3 HALLUCINATION REGULATOR422
423 Recognizing that hallucinations can have positive effects in certain scenarios like creative writing
424 (Jiang et al., 2024b), it is important to have a controllable generation of hallucinations. However,
425 existing methods exhibit unstable hallucination control capabilities. Detailed experimental results
426 are provided in Appendix D.8. Hence, we conduct experiments on the edit strength hyperparameter
427 α in formulation 4 to investigate its critical role in hallucination control for LVLMs. As shown
428 in Figure 3, we conduct experiments with different values of α , ranging from -0.7 to 1.0. It can
429 be found that a positive α value can mitigate hallucination at both sentence-level and object-level
430 granularities, and the reduction of hallucination increases with higher values. Conversely, negative
431 α values demonstrate a proportional amplification effect on hallucination rates, with lower values
432 inducing stronger hallucinatory responses. From the figure, it can be observed that our method has
433 excellent controllability in hallucination generation.

432 Table 4: Ablation study on the impact of encoder architecture and the Router module. Results show
 433 the effects on hallucination mitigation performance and computational cost.

434

	Semantic encoder	Hallucinatory encoder	Router	$\text{CHAIR}_S \downarrow$	$\text{CHAIR}_I \downarrow$	TFLOPs \downarrow
1				51.3	16.8	10.23
2		✓		37.0	12.2	-
3			✓	48.6	13.0	-
4	✓		✓	30.4	9.5	16.23
5	✓	✓	✓	30.2	9.7	11.81

441



455 Figure 4: Some examples of generative and discriminative tasks on the MSCOCO dataset, with
 456 hallucinated content highlighted in red and newly added correct content displayed in green.
 457

458

459
460

5.4 ABLATION STUDY

461

We conduct ablation studies on CHAIR using LLaVA-1.5 to validate each module’s contribution. As shown in Table 4, the original model’s results are provided first. Adding only the semantic encoder or hallucinatory encoder individually yields limited gains. Combining both achieves the lowest hallucination rate, demonstrating their complementary roles. Furthermore, integrating the Router reduces computational cost by $\sim 30\%$ without performance loss, underscoring its efficiency. These results confirm the necessity of both encoders for effective hallucination mitigation and the Router’s role in maintaining efficiency.

472

473
474

5.5 QUALITATIVE EVALUATION

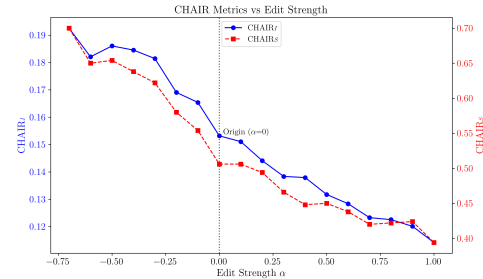
475

To better illustrate the effectiveness of our method, Fig. 4 presents representative examples from both generative tasks and discriminative tasks on the MSCOCO dataset. Hallucinated content in the figure is highlighted in red. It can be observed that our method eliminates hallucinations and provides a more accurate interpretation of the image. More results are provided in the Appendix E.

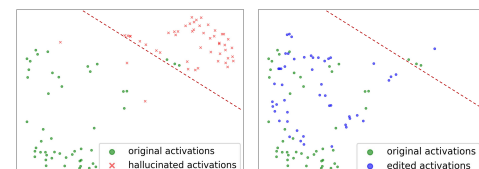
479

480
481
482
483
484
485

To demonstrate our method’s effectiveness in suppressing hallucination within the representation space, Figure 5 compares distributions of non-hallucinated (green), hallucinated (red), and edited (blue) feature. Non-hallucinated features are extracted using the image and its ground-truth caption. Following Wang et al. (2024), we introduce hallucination into features via a disturbed prompt and hallu-



476 Figure 3: Control hallucination generation via
 477 α .



478 Figure 5: Distribution of original, hallucinated,
 479 and edited representations.

486 cinated caption to avoid image perturbation bias. Edited representations result from applying our
 487 Editor to hallucinated ones. The left subfigure shows clear separation between hallucinated and
 488 non-hallucinated clusters in the hallucinatory subspace. On the right, edited representations shift
 489 toward the non-hallucinated cluster and exhibit overlap and converge, confirming that our editing
 490 effectively reduces hallucination.

492 5.6 COMPATIBILITY WITH STEERING-BASED METHODS

494 Several steering-based methods exist for hallucination mitigation. For example, Nullu (Yang et al.,
 495 2025) operates by editing model weights and Projectaway (Jiang et al.) removes hallucinations from
 496 image features. In contrast, our method focuses on the textual feature space and further making
 497 fine-grained editing decisions per token. Hence, our approach can be integrated with other steering-
 498 based methods, offering a composite solution. Following the experimental settings of these methods,
 499 we evaluate the combined performance using the CHAIR metric across different max new token
 500 constraints. As shown in Table 5 and Table 6, our method can be combined with steering-based
 501 methods to yield stronger hallucination suppression.

503 Table 5: Evaluation results on the CHAIR
 504 with Max New Tokens set to 512.

Method	CHAIR _S ↓	CHAIR _I ↓
LLaVA-1.5-7B	51.3	16.8
+Projectaway	43.8	12.5
+Ours	30.2	9.7
+Ours & Projectaway	27.6	8.3

503 Table 6: Evaluation results on the CHAIR
 504 with Max New Tokens set to 64.

Method	CHAIR _S ↓	CHAIR _I ↓
LLaVA-1.5-7B	20.4	6.2
+Nullu	17.0	5.9
+Ours	15.2	5.4
+Ours & Nullu	13.2	4.6

513 5.7 EVALUATION ON GENERAL CAPABILITIES

515 We evaluate the general capabilities of the model equipped HIRE, using LLaVA-1.5-7B as a repre-
 516 sentative model on two challenging benchmarks: MME (Yin et al., 2024a) and SEED-Bench (Li
 517 et al., 2023a). As shown in Table 7, it can be observed that our method preserves the model’s general
 518 capabilities on these benchmarks.

520 Table 7: Comparison of general capabilities on MME and SEED-Bench.

Method	MME ↑	SEED ↑
LLaVA-1.5 7B	1751.64	64.3
+Ours	1751.99	63.8

527 6 CONCLUSION AND LIMITATIONS

530 In this paper, we propose a novel adaptive feature-editing framework that dynamically detects and
 531 calibrates hidden-layer activations to either suppress or enhance hallucinations, forming flexible,
 532 input-aware workflows. Our method operates in a single inference pass without updating parameters
 533 of LVLMs, offering exceptional efficiency while maintaining strong performance. It is also easily
 534 extendable to tasks requiring flexible control over hallucinations. We expect that this work will
 535 provide a general, practical paradigm for mitigating hallucination across diverse scenarios.

536 Despite these advantages, we note a limitation of the current framework. Our method employs all
 537 tokens and layers for training, a process that can be susceptible to noise. Training selectively on the
 538 most critical hidden states presents a significant opportunity for enhancing data efficiency. This work,
 539 as an initial step, aimed primarily at validating the feasibility of the proposed editing paradigm. We
 will explore the aforementioned direction in future work.

540 REFERENCES
541

542 Wenbin An, Feng Tian, Sicong Leng, Jiahao Nie, Haonan Lin, QianYing Wang, Guang Dai, Ping
543 Chen, and Shijian Lu. Agla: Mitigating object hallucinations in large vision-language models with
544 assembly of global and local attention. *arXiv preprint arXiv:2406.12718*, 2024.

545 Stanislaw Antol, Aishwarya Agrawal, Jiasen Lu, Margaret Mitchell, Dhruv Batra, C Lawrence Zitnick,
546 and Devi Parikh. Vqa: Visual question answering. In *Proceedings of the IEEE international
547 conference on computer vision*, pp. 2425–2433, 2015.

548 Amos Azaria and Tom Mitchell. The internal state of an LLM knows when it’s lying. In
549 Houda Bouamor, Juan Pino, and Kalika Bali (eds.), *Findings of the Association for Compu-
550 tational Linguistics: EMNLP 2023*, pp. 967–976, Singapore, December 2023. Association
551 for Computational Linguistics. doi: 10.18653/v1/2023.findings-emnlp.68. URL <https://aclanthology.org/2023.findings-emnlp.68/>.

552 Jinze Bai, Shuai Bai, Yunfei Chu, Zeyu Cui, Kai Dang, Xiaodong Deng, Yang Fan, Wenbin Ge,
553 Yu Han, Fei Huang, et al. Qwen technical report. *arXiv preprint arXiv:2309.16609*, 2023a.

554 Jinze Bai, Shuai Bai, Shusheng Yang, Shijie Wang, Sinan Tan, Peng Wang, Junyang Lin, Chang Zhou,
555 and Jingren Zhou. Qwen-vl: A versatile vision-language model for understanding, localization,
556 text reading, and beyond, 2023b. URL <https://arxiv.org/abs/2308.12966>.

557 Shuai Bai, Keqin Chen, Xuejing Liu, Jialin Wang, Wenbin Ge, Sibo Song, Kai Dang, Peng Wang,
558 Shijie Wang, Jun Tang, et al. Qwen2. 5-vl technical report. *arXiv preprint arXiv:2502.13923*,
559 2025.

560 Tom Brown, Benjamin Mann, Nick Ryder, Melanie Subbiah, Jared D Kaplan, Prafulla Dhariwal,
561 Arvind Neelakantan, Pranav Shyam, Girish Sastry, Amanda Askell, et al. Language models are
562 few-shot learners. *Advances in neural information processing systems*, 33:1877–1901, 2020.

563 Liang Chen, Haozhe Zhao, Tianyu Liu, Shuai Bai, Junyang Lin, Chang Zhou, and Baobao Chang.
564 An image is worth 1/2 tokens after layer 2: Plug-and-play inference acceleration for large vision-
565 language models. In *European Conference on Computer Vision*, pp. 19–35. Springer, 2024a.

566 Nuo Chen, Ning Wu, Shining Liang, Ming Gong, Linjun Shou, Dongmei Zhang, and Jia Li. Is
567 bigger and deeper always better? probing llama across scales and layers, 2024b. URL <https://arxiv.org/abs/2312.04333>.

568 Zhongzhi Chen, Xingwu Sun, Xianfeng Jiao, Fengzong Lian, Zhanhui Kang, Di Wang, and
569 Chengzhong Xu. Truth forest: Toward multi-scale truthfulness in large language models through
570 intervention without tuning. In *Proceedings of the AAAI Conference on Artificial Intelligence*,
571 volume 38, pp. 20967–20974, 2024c.

572 Wei-Lin Chiang, Zhuohan Li, Zi Lin, Ying Sheng, Zhanghao Wu, Hao Zhang, Lianmin Zheng,
573 Siyuan Zhuang, Yonghao Zhuang, Joseph E. Gonzalez, Ion Stoica, and Eric P. Xing. Vicuna: An
574 open-source chatbot impressing gpt-4 with 90%* chatgpt quality, March 2023. URL <https://lmsys.org/blog/2023-03-30-vicuna/>.

575 Wenliang Dai, Junnan Li, Dongxu Li, Anthony Meng Huat Tiong, Junqi Zhao, Weisheng Wang,
576 Boyang Li, Pascale Fung, and Steven Hoi. Instructblip: Towards general-purpose vision-language
577 models with instruction tuning, 2023. URL <https://arxiv.org/abs/2305.06500>.

578 Alexey Dosovitskiy, Lucas Beyer, Alexander Kolesnikov, Dirk Weissenborn, Xiaohua Zhai, Thomas
579 Unterthiner, Mostafa Dehghani, Matthias Minderer, Georg Heigold, Sylvain Gelly, et al. An
580 image is worth 16x16 words: Transformers for image recognition at scale. *arXiv preprint
581 arXiv:2010.11929*, 2020.

582 NR Draper. *Applied regression analysis*. McGraw-Hill. Inc, 1998.

583 Jinhao Duan, Fei Kong, Hao Cheng, James Diffenderfer, Bhavya Kailkhura, Lichao Sun, Xiaofeng
584 Zhu, Xiaoshuang Shi, and Kaidi Xu. Truthprint: Mitigating lvlm object hallucination via latent
585 truthful-guided pre-intervention. *arXiv preprint arXiv:2503.10602*, 2025.

594 Alessandro Favero, Luca Zancato, Matthew Trager, Siddharth Choudhary, Pramuditha Perera,
 595 Alessandro Achille, Ashwin Swaminathan, and Stefano Soatto. Multi-modal hallucination control
 596 by visual information grounding. In *Proceedings of the IEEE/CVF Conference on Computer Vision*
 597 and *Pattern Recognition*, pp. 14303–14312, 2024.

598
 599 Yuhan Fu, Ruobing Xie, Xingwu Sun, Zhanhui Kang, and Xirong Li. Mitigating hallucination in
 600 multimodal large language model via hallucination-targeted direct preference optimization. *arXiv*
 601 preprint *arXiv:2411.10436*, 2024.

602 MD Zakir Hossain, Ferdous Sohel, Mohd Fairuz Shiratuddin, and Hamid Laga. A comprehensive
 603 survey of deep learning for image captioning. *ACM Computing Surveys (CsUR)*, 51(6):1–36, 2019.
 604

605 Qidong Huang, Xiaoyi Dong, Pan Zhang, Bin Wang, Conghui He, Jiaqi Wang, Dahua Lin, Weiming
 606 Zhang, and Nenghai Yu. Opera: Alleviating hallucination in multi-modal large language models
 607 via over-trust penalty and retrospection-allocation. In *Proceedings of the IEEE/CVF Conference*
 608 on *Computer Vision and Pattern Recognition*, pp. 13418–13427, 2024.

609 Drew A Hudson and Christopher D Manning. Gqa: A new dataset for real-world visual reasoning
 610 and compositional question answering. In *Proceedings of the IEEE/CVF conference on computer*
 611 *vision and pattern recognition*, pp. 6700–6709, 2019.
 612

613 Fushuo Huo, Wenchao Xu, Zhong Zhang, Haozhao Wang, Zhicheng Chen, and Peilin Zhao. Self-
 614 introspective decoding: Alleviating hallucinations for large vision-language models. *arXiv preprint*
 615 *arXiv:2408.02032*, 2024.

616 Chaoya Jiang, Haiyang Xu, Mengfan Dong, Jiaxing Chen, Wei Ye, Ming Yan, Qinghao Ye, Ji Zhang,
 617 Fei Huang, and Shikun Zhang. Hallucination augmented contrastive learning for multimodal large
 618 language model. In *Proceedings of the IEEE/CVF Conference on Computer Vision and Pattern*
 619 *Recognition*, pp. 27036–27046, 2024a.
 620

621 Nicholas Jiang, Anish Kachinthaya, Suzanne Petryk, and Yossi Gandelsman. Interpreting and
 622 editing vision-language representations to mitigate hallucinations. In *The Thirteenth International*
 623 *Conference on Learning Representations*.

624 Xuhui Jiang, Yuxing Tian, Fengrui Hua, Chengjin Xu, Yuanzhuo Wang, and Jian Guo. A survey on
 625 large language model hallucination via a creativity perspective. *arXiv preprint arXiv:2402.06647*,
 626 2024b.
 627

628 Diederik P Kingma and Jimmy Ba. Adam: A method for stochastic optimization. *arXiv preprint*
 629 *arXiv:1412.6980*, 2014.

630 Ranjay Krishna, Yuke Zhu, Oliver Groth, Justin Johnson, Kenji Hata, Joshua Kravitz, Stephanie
 631 Chen, Yannis Kalantidis, Li-Jia Li, David A Shamma, et al. Visual genome: Connecting language
 632 and vision using crowdsourced dense image annotations. *International journal of computer vision*,
 633 123(1):32–73, 2017.
 634

635 Sicong Leng, Hang Zhang, Guanzheng Chen, Xin Li, Shijian Lu, Chunyan Miao, and Lidong Bing.
 636 Mitigating object hallucinations in large vision-language models through visual contrastive decod-
 637 ing. In *Proceedings of the IEEE/CVF Conference on Computer Vision and Pattern Recognition*,
 638 pp. 13872–13882, 2024.

639 Bohao Li, Rui Wang, Guangzhi Wang, Yuying Ge, Yixiao Ge, and Ying Shan. Seed-bench: Bench-
 640 marking multimodal llms with generative comprehension. *arXiv preprint arXiv:2307.16125*,
 641 2023a.
 642

643 Junnan Li, Dongxu Li, Silvio Savarese, and Steven Hoi. BLIP-2: Bootstrapping language-image
 644 pre-training with frozen image encoders and large language models. In Andreas Krause, Emma
 645 Brunskill, Kyunghyun Cho, Barbara Engelhardt, Sivan Sabato, and Jonathan Scarlett (eds.),
 646 *Proceedings of the 40th International Conference on Machine Learning*, volume 202 of *Pro-
 647 ceedings of Machine Learning Research*, pp. 19730–19742. PMLR, 23–29 Jul 2023b. URL
<https://proceedings.mlr.press/v202/li23q.html>.

648 Kenneth Li, Oam Patel, Fernanda Viégas, Hanspeter Pfister, and Martin Wattenberg. Inference-time
 649 intervention: Eliciting truthful answers from a language model. *Advances in Neural Information
 650 Processing Systems*, 36:41451–41530, 2023c.

651

652 Qing Li, Jiahui Geng, Chenyang Lyu, Derui Zhu, Maxim Panov, and Fakhri Karray. Reference-free
 653 hallucination detection for large vision-language models, 2024. URL <https://arxiv.org/abs/2408.05767>.

654

655 Yifan Li, Yifan Du, Kun Zhou, Jinpeng Wang, Wayne Xin Zhao, and Ji-Rong Wen. Evaluating object
 656 hallucination in large vision-language models. *arXiv preprint arXiv:2305.10355*, 2023d.

657

658 Tsung-Yi Lin, Michael Maire, Serge Belongie, James Hays, Pietro Perona, Deva Ramanan, Piotr
 659 Dollár, and C Lawrence Zitnick. Microsoft coco: Common objects in context. In *Computer vision–
 660 ECCV 2014: 13th European conference, zurich, Switzerland, September 6–12, 2014, proceedings,
 661 part v 13*, pp. 740–755. Springer, 2014.

662 Fuxiao Liu, Kevin Lin, Linjie Li, Jianfeng Wang, Yaser Yacoob, and Lijuan Wang. Mitigating
 663 hallucination in large multi-modal models via robust instruction tuning. In *ICLR*, 2024a.

664

665 Haotian Liu, Chunyuan Li, Yuheng Li, and Yong Jae Lee. Improved baselines with visual instruction
 666 tuning. In *Proceedings of the IEEE/CVF Conference on Computer Vision and Pattern Recognition*,
 667 pp. 26296–26306, 2024b.

668 Sheng Liu, Haotian Ye, and James Zou. Reducing hallucinations in large vision-language models via
 669 latent space steering. In *The Thirteenth International Conference on Learning Representations*,
 670 2025.

671

672 Ilya Loshchilov and Frank Hutter. Decoupled weight decay regularization. In *International Conference
 673 on Learning Representations*.

674

675 Jiaying Lu, Jinmeng Rao, Kezhen Chen, Xiaoyuan Guo, Yawen Zhang, Baochen Sun, Carl Yang, and
 676 Jie Yang. Evaluation and enhancement of semantic grounding in large vision-language models.
 677 *arXiv preprint arXiv:2309.04041*, 2023.

678 Pan Lu, Swaroop Mishra, Tanglin Xia, Liang Qiu, Kai-Wei Chang, Song-Chun Zhu, Oyvind Tafjord,
 679 Peter Clark, and Ashwin Kalyan. Learn to explain: Multimodal reasoning via thought chains for
 680 science question answering. *Advances in Neural Information Processing Systems*, 35:2507–2521,
 681 2022.

682 Sheng Luo, Wei Chen, Wanxin Tian, Rui Liu, Luanxuan Hou, Xiubao Zhang, Haifeng Shen, Ruiqi
 683 Wu, Shuyi Geng, Yi Zhou, et al. Delving into multi-modal multi-task foundation models for road
 684 scene understanding: From learning paradigm perspectives. *IEEE Transactions on Intelligent
 685 Vehicles*, 2024.

686

687 Avshalom Manevich and Reut Tsarfaty. Mitigating hallucinations in large vision-language models
 688 (lvm) via language-contrastive decoding (lcd). In *Findings of the Association for Computational
 689 Linguistics ACL 2024*, pp. 6008–6022, 2024.

690

691 Yu Meng, Mengzhou Xia, and Danqi Chen. Simpo: Simple preference optimization with a reference-
 692 free reward. *Advances in Neural Information Processing Systems*, 37:124198–124235, 2024.

693

694 Aaron van den Oord, Yazhe Li, and Oriol Vinyals. Representation learning with contrastive predictive
 695 coding. *arXiv preprint arXiv:1807.03748*, 2018.

696

697 Kishore Papineni, Salim Roukos, Todd Ward, and Wei-Jing Zhu. Bleu: a method for automatic
 698 evaluation of machine translation. In *Proceedings of the 40th annual meeting of the Association
 699 for Computational Linguistics*, pp. 311–318, 2002.

700

701 Alec Radford, Jong Wook Kim, Chris Hallacy, Aditya Ramesh, Gabriel Goh, Sandhini Agarwal,
 702 Girish Sastry, Amanda Askell, Pamela Mishkin, Jack Clark, et al. Learning transferable visual
 703 models from natural language supervision. In *International conference on machine learning*, pp.
 704 8748–8763. PMLR, 2021.

702 Rafael Rafailov, Archit Sharma, Eric Mitchell, Christopher D Manning, Stefano Ermon, and Chelsea
 703 Finn. Direct preference optimization: Your language model is secretly a reward model. *Advances*
 704 *in Neural Information Processing Systems*, 36:53728–53741, 2023.

705 Anna Rohrbach, Lisa Anne Hendricks, Kaylee Burns, Trevor Darrell, and Kate Saenko. Object
 706 hallucination in image captioning. *arXiv preprint arXiv:1809.02156*, 2018.

708 Dustin Schwenk, Apoorv Khandelwal, Christopher Clark, Kenneth Marino, and Roozbeh Mottaghi.
 709 A-okvqa: A benchmark for visual question answering using world knowledge. In *European*
 710 *conference on computer vision*, pp. 146–162. Springer, 2022.

711 Wei Suo, Ji Ma, Mengyang Sun, Lin Yuanbo Wu, Peng Wang, and Yanning Zhang. Pruning all-
 712 rounder: Rethinking and improving inference efficiency for large vision language models. *arXiv*
 713 *preprint arXiv:2412.06458*, 2024.

715 Wei Suo, Lijun Zhang, Mengyang Sun, Lin Yuanbo Wu, Peng Wang, and Yanning Zhang. Octopus:
 716 Alleviating hallucination via dynamic contrastive decoding. *arXiv preprint arXiv:2503.00361*,
 717 2025.

718 Hugo Touvron, Thibaut Lavril, Gautier Izacard, Xavier Martinet, Marie-Anne Lachaux, Timothée
 719 Lacroix, Baptiste Rozière, Naman Goyal, Eric Hambro, Faisal Azhar, et al. Llama: Open and
 720 efficient foundation language models. *arXiv preprint arXiv:2302.13971*, 2023.

722 Ashish Vaswani, Noam Shazeer, Niki Parmar, Jakob Uszkoreit, Llion Jones, Aidan N Gomez, Łukasz
 723 Kaiser, and Illia Polosukhin. Attention is all you need. *Advances in neural information processing*
 724 *systems*, 30, 2017.

725 Junyang Wang, Yuhang Wang, Guohai Xu, Jing Zhang, Yukai Gu, Haitao Jia, Jiaqi Wang, Haiyang
 726 Xu, Ming Yan, Ji Zhang, et al. Amber: An llm-free multi-dimensional benchmark for mllms
 727 hallucination evaluation. *arXiv preprint arXiv:2311.07397*, 2023.

728 Sudong Wang, Yunjian Zhang, Yao Zhu, Jianing Li, Zizhe Wang, Yanwei Liu, and Xiangyang Ji.
 729 Towards understanding how knowledge evolves in large vision-language models. In *Proceedings*
 730 *of the Computer Vision and Pattern Recognition Conference*, pp. 29858–29868, 2025.

732 Xintong Wang, Jingheng Pan, Liang Ding, and Chris Biemann. Mitigating hallucinations in large
 733 vision-language models with instruction contrastive decoding. *arXiv preprint arXiv:2403.18715*,
 734 2024.

735 Sangmin Woo, Donguk Kim, Jaehyuk Jang, Yubin Choi, and Changick Kim. Don’t miss the forest
 736 for the trees: Attentional vision calibration for large vision language models. *arXiv preprint*
 737 *arXiv:2405.17820*, 2024.

739 Qiong Wu, Wei Yu, Yiyi Zhou, Shubin Huang, Xiaoshuai Sun, and Rongrong Ji. Parameter and
 740 computation efficient transfer learning for vision-language pre-trained models. *Advances in Neural*
 741 *Information Processing Systems*, 36:41034–41050, 2023.

742 Yun Xing, Yiheng Li, Ivan Laptev, and Shijian Lu. Mitigating object hallucination via concentric
 743 causal attention. *Advances in Neural Information Processing Systems*, 37:92012–92035, 2024.

745 Le Yang, Ziwei Zheng, Boxu Chen, Zhengyu Zhao, Chenhao Lin, and Chao Shen. Nullu: Mitigating
 746 object hallucinations in large vision-language models via halluspace projection. In *Proceedings of*
 747 *the Computer Vision and Pattern Recognition Conference*, pp. 14635–14645, 2025.

748 Shukang Yin, Chaoyou Fu, Sirui Zhao, Ke Li, Xing Sun, Tong Xu, and Enhong Chen. A survey on
 749 multimodal large language models. *National Science Review*, 11(12):nwae403, 2024a.

751 Shukang Yin, Chaoyou Fu, Sirui Zhao, Tong Xu, Hao Wang, Dianbo Sui, Yunhang Shen, Ke Li, Xing
 752 Sun, and Enhong Chen. Woodpecker: Hallucination correction for multimodal large language
 753 models. *Science China Information Sciences*, 67(12):220105, 2024b.

754 Shaolei Zhang, Tian Yu, and Yang Feng. Truthx: Alleviating hallucinations by editing large language
 755 models in truthful space. In *Proceedings of the 62nd Annual Meeting of the Association for*
Computational Linguistics (Volume 1: Long Papers), pp. 8908–8949, 2024.

756 Zhiyuan Zhao, Bin Wang, Linke Ouyang, Xiaoyi Dong, Jiaqi Wang, and Conghui He. Beyond
757 hallucinations: Enhancing lylms through hallucination-aware direct preference optimization. *arXiv*
758 *preprint arXiv:2311.16839*, 2023.

759 Baichuan Zhou, Ying Hu, Xi Weng, Junlong Jia, Jie Luo, Xien Liu, Ji Wu, and Lei Huang. Tinyllava:
760 A framework of small-scale large multimodal models. *arXiv preprint arXiv:2402.14289*, 2024.

762 Deyao Zhu, Jun Chen, Xiaoqian Shen, Xiang Li, and Mohamed Elhoseiny. Minigpt-4: En-
763 hancing vision-language understanding with advanced large language models. *arXiv preprint*
764 *arXiv:2304.10592*, 2023.

765

766

767

768

769

770

771

772

773

774

775

776

777

778

779

780

781

782

783

784

785

786

787

788

789

790

791

792

793

794

795

796

797

798

799

800

801

802

803

804

805

806

807

808

809

810 A DETAILED EXPERIMENTAL SETTINGS
811812 A.1 VISUAL PERTURBATION METHODS
813

814 We follow VCD (Leng et al., 2024) to apply visual perturbations by introducing noise to images. For
815 LLaVA-1.5, we set the noise step to its maximum value of 999, which lies within its supported range
816 of 0–999. For InstructBLIP, considering that the Q-former module relies on interactions between
817 textual and visual inputs, excessively corrupted images can introduce unwanted degradation into the
818 representations. To mitigate this, we limit the noise step to 600.

819 B LICENSE OF ASSETS
820

822 LLaVA-1.5 (Liu et al., 2024b) is available under the Apache-2.0 License and InstructBLIP (Dai et al.,
823 2023) is available under BSD-3-Clause License. CHAIR is under the BSE 2-Clause License. POPE
824 is available under the MIT License and AMBER is available under Apache-2.0 License.

826 C EVALUATION METRIC
827

828 **AMBER.** We follow the experimental setup in (Suo et al., 2025). In the generative task of AMBER,
829 we report four metrics: CHAIR, Cover, Hal, and Cog.

831 *CHAIR* measures the proportion of objects mentioned in the generated sentences but not present in the
832 ground-truth labels. Specifically, given the list of generated objects $G_{obj} = \{obj_1^G, obj_2^G, \dots, obj_n^G\}$
833 and the list of annotated objects $A_{obj} = \{obj_1^A, obj_2^A, \dots, obj_n^A\}$. *CHAIR* is calculated by the
834 following formula:

$$835 \quad 836 \quad 837 \quad CHAIR = 1 - \frac{\text{len}(G_{obj} \cap A_{obj})}{G_{obj}}. \quad (9)$$

838 *Cover* measures the ratio of between the correctly mentioned objects in responses and the total num
839 of objects in the annotations:

$$841 \quad 842 \quad 843 \quad Cover = \frac{\text{len}(G_{obj} \cap A_{obj})}{\text{len}(A_{obj})}. \quad (10)$$

844 *Hal* indicates whether a response contains hallucination. For each response, Hal is defined as 1 when
845 the CHAIR score is greater than 0, and 0 otherwise, as shown below:

$$847 \quad 848 \quad Hal = \mathbb{I}(CHAIR > 0), \quad (11)$$

849 **Cog** measures the alignment between model-generated hallucinations and those identified by hu
850 man cognition. Specifically, AMBER defines a target set of hallucinated objects as $H_{obj} =$
851 $\{obj_1^H, obj_2^H, \dots, obj_m^H\}$. The Cog score is computed as the proportion of hallucinated objects
852 generated by the model that also appear in the human-annotated set, as shown below:

$$854 \quad 855 \quad 856 \quad Cog = \frac{|G_{obj} \cap H_{obj}|}{|G_{obj}|}. \quad (12)$$

857 D ADDITIONAL EXPERIMENTS
858859 D.1 EDIT LAYERS FOR HIRE’s EDITOR
860

862 To investigate the influence of different editing layer, Table 8 shows the hallucination mitigation
863 performance with three different editing layer sets, where shallow layers represent the editing layers
of 0~9, middle layers represent the editing layers of 10~19, deep layers represent the editing layers

864 Table 8: Evaluating the impact of editing different layers on the CHAIR benchmark.
865

866 Edit layer	867 $\text{CHAIR}_S \downarrow$	868 $\text{CHAIR}_I \downarrow$
869 baseline	870 51.3	871 16.8
872 shallow (0~9)	873 42.0	874 13.0
875 middle (10~19)	876 36.0	877 10.7
878 deep (20~29)	879 46.8	880 14.1
881 HIRE (0~31)	882 30.2	883 9.7

873 Table 9: Performance of different router strategies evaluated by hallucination (CHAIR) and text
874 quality (BLEU).
875

876 Router type	877 $\text{CHAIR}_S \downarrow$	878 $\text{CHAIR}_I \downarrow$	879 BLEU \uparrow	880 training time \downarrow
881 LLaVA-1.5	882 51.3	883 16.8	884 17.47	885 -
886 I (a unified router)	887 30.6	888 9.6	889 20.53	890 11h
891 II (layer-specific routers)	892 30.4	893 9.6	894 20.65	895 14h
896 III (initial embedding-based decision)	897 46.2	898 12.9	899 16.93	900 8h
901 Ours (first layer embedding-based decision)	902 30.2	903 9.7	904 20.59	905 8h

884 of 20~29. The results indicate that editing the middle layers plays the most significant role in
885 mitigating hallucinations, while editing shallow layers has a moderate effect. Editing deep layers,
886 however, shows minimal contribution to performance gains. However, editing all layers achieves
887 superior performance compared to editing only partial layers.

889 D.2 EXPERIMENTS ON LAYER-WISE CONTROL

890 We conduct comparative studies about router decision strategies, comparing with: (I) **a unified router**
891 shared across all tokens and layers; (II) **layer-specific routers**: each layer owns an independent
892 router; (III) **initial embedding-based decision**: the router determines editing decisions for all
893 subsequent layers based solely on the input embedding of the LVLM. To evaluate the quality of
894 responses generated by our method, we further incorporate the BLEU metric (Papineni et al., 2002)
895 (where higher scores indicate better sentence quality) to assess semantic integrity and coherence.
896 The corresponding results are summarized in Table 9. We observe that both Strategy I and Strategy
897 II achieve performance comparable to our first layer embedding-based decision approach in terms
898 of hallucination mitigation. However, our method requires only a single router decision during the
899 forward pass, leading to a reduction in training time by approximately $\sim 30\%$. Furthermore, compared
900 to Strategy III, our first layer-based decision mechanism more effectively reduces hallucinations.
901 This improvement may be attributed to the fact that the first-layer representations process the input
902 embeddings into activations that are more discriminative for hallucination detection.

903 D.3 COMPARISON OF DIVERSE HALLUCINATION INDUCTION METHODS

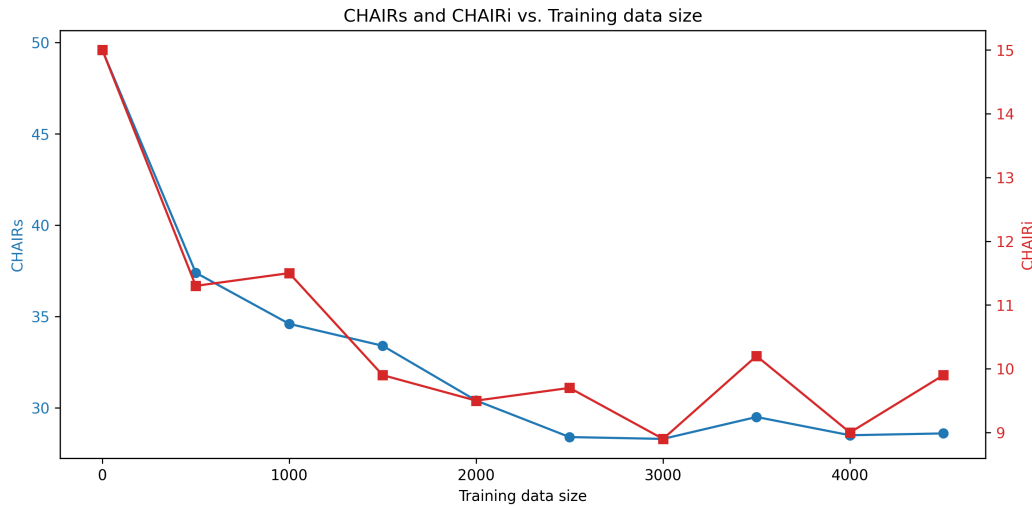
904 We conduct a comparative experiment to validate the robustness of our method to different hallu-
905 cination induction approaches. Specifically, we introduce hallucinations by providing the model
906 with confusing instructions (Wang et al., 2024) during training. Table 10 shows that perturbing the
907 instructions given to LVLMs can be effectively integrated with our approach, yielding comparable
908 performance in hallucination mitigation. This indicates that our method is robust against different
909 hallucination-inducing strategies.

910 D.4 DATA SIZE FOR HIRE’s EDITOR TRAINING

911 To investigate the impact of training data size on model performance, we report hallucination
912 mitigation results under varying training scales on the CHAIR benchmark. As shown in Fig. 6, the
913 model’s ability to mitigate hallucinations plateaus when the dataset size reaches about 2500 samples.
914 As a result, performance cannot be further improved by large-scale training beyond this range. We
915 argue that our approach requires no adjustments to the original LVLM parameters. Rather, it learns
916

918 Table 10: CHAIR evaluation of HIRE trained with different hallucination induction methods.
919

Method	$\text{CHAIR}_S \downarrow$	$\text{CHAIR}_I \downarrow$
LLaVA-1.5	51.3	16.8
Instruction perturbation	32.4	8.7
Visual perturbation	30.2	9.7

935 Figure 6: Performance of HIRE on CHAIR benchmark under different training data sizes.
936943
944 an editing direction by training an editor and a router (0.05B parameters). Therefore, only a small
945 number of samples is required to achieve effective hallucination mitigation with our method.
946950 D.5 HYPERPARAMETER SENSITIVITY ANALYSIS
951953 To validate the training stability, we conduct additional experiments by retraining the model with
954 different learning rates and scaling factors β , all without using a learning rate scheduler. As shown in
955 Table 11, it can be found that our method shows low sensitivity to hyperparameters. Although certain
956 settings can yield better performance, our primary focus is not to achieve SOTA results through
957 hyperparameter tuning. Instead, we aim to provide the community with a novel perspective to rethink
958 feature-level hallucination mitigation.
959960 Table 11: Analysis of training stability under different hyperparameters.
961

Setting	$\text{CHAIRs} \downarrow$	$\text{CHAIRi} \downarrow$
<i>Varying Learning Rate.</i>		
LLaVA-1.5-7B	51.3	16.8
+Ours (1e-3)	30.2	9.7
5e-4	32.4	12.1
5e-5	33.4	10.2
<i>Varying Scaling Factor β.</i>		
0.05	31.6	10.1
+Ours (0.1)	30.2	9.7
0.15	32.4	10.3

972
973
974 Table 12: Evaluation on CHAIR and AMBER across model types and scales
975
976
977
978
979
980
981

Model	CHAIR		AMBER			
	CHAIR _s ↓	CHAIR _i ↓	CHAIR ↓	Cover. ↑	Cog. ↓	HalRate ↓
Qwen-2.5-VL	46.2	9.6	8.8	59.9	3.4	46.6
Qwen-2.5-VL+Ours	35.6	8.1	6.5	60.3	2.1	36.8
TinyLLaVA-1.5B	58.6	17.5	11.2	50.8	6.2	48.0
TinyLLaVA-1.5B+Ours	36.6	11.7	8.6	48.7	2.6	35.6
LLaVA-1.5-13B	43.8	12.3	6.3	51.2	3.1	30.9
LLaVA-1.5-13B+Ours	29.8	8.2	4.6	49.0	1.7	22.0

982
983 Table 13: More results on the GQA and A-OKVQA datasets of POPE.
984
985
986
987
988
989
990
991
992
993
994
995

Dataset	Method	Random		Popular		Adversarial		All	
		Acc↑	F1↑	Acc↑	F1↑	Acc↑	F1↑	Acc↑	F1↑
A-OKVQA	LLaVA-1.5	84.93	84.07	80.90	80.64	74.80	75.59	80.21	80.10
	+VCD	85.53	85.12	81.17	81.46	75.03	76.72	80.58	81.10
	+M3ID	85.06	84.30	80.90	80.77	74.80	76.15	80.25	80.41
	+AVISC	87.33	86.14	85.03	84.03	79.27	79.16	83.88	83.11
	+Ours	88.90	89.20	86.50	86.52	78.07	79.70	84.49	85.14
GQA	LLaVA-1.5	84.80	84.16	79.37	79.64	76.00	76.89	80.08	80.23
	+VCD	85.63	85.38	78.73	79.78	76.40	78.15	80.25	81.10
	+M3ID	84.80	84.23	79.23	79.63	75.83	76.93	79.95	80.26
	+AVISC	87.40	86.21	83.33	82.54	80.37	80.00	83.70	82.92
	+Ours	88.87	89.21	84.67	85.21	80.63	82.07	84.72	85.50

996
997
998 D.6 EVALUATING GENERALIZATION ABILITY ON DIVERSE MODELS AND DATASETS
9991000 To validate the generalization ability of our method, we present more experimental results on Qwen-
1001 2.5-VL-3B (Bai et al., 2025) and different scales of LLaVA series (Zhou et al., 2024; Liu et al.,
1002 2024b). It can be observed in Table 12 that our method still performs well across different types and
1003 scales of LVLMs.1004 We further present evaluation results on the GQA (Hudson & Manning, 2019) and A-OKVQA
1005 (Schwenk et al., 2022) datasets under the POPE benchmark in Table 13, comparing against previously
1006 reported results from Woo et al. (2024). Our method achieves consistent improvements in both
1007 accuracy and F1 score across these datasets.1008 We further conduct a cross-dataset experiment to evaluate the generalization ability of our method.
1009 Specifically, we randomly select 2,000 samples from Visual Genome (Krishna et al., 2017) (excluding
1010 overlaps with MSCOCO) to retrain our model and evaluate it on the MSCOCO dataset. Results in
1011 Table 14 show that our model maintains strong hallucination suppression performance even when
1012 trained on Visual Genome.1013
1014 D.7 METHOD STABILITY ANALYSIS1015 To evaluate the stability of our method, we train the model five times with distinct random seeds and
1016 assess its performance on the CHAIR benchmark. As shown in Table 15, our approach consistently
1017 achieves stable results across different runs. On average, our method reduces CHAIR_S and CHAIR_I
1018 by 20.8 and 7.4, respectively, with variances as low as 1.3 and 0.31. These results demonstrate the
1019 high stability and reliability of our approach.1020
1021 D.8 HALLUCINATION CONTROLLABILITY OF EXISTING METHODS
10221023 We focus on evaluating the hallucination control capability of post-hoc methods, specifically Con-
1024 trastive Decoding (CD) and feature steering methods, as retraining-based methods lack this property.
1025 The evaluation is conducted on the CHAIR benchmark under a controlled setting (max new tokens
= 512) using VCD Leng et al. (2024) and VTI Liu et al. (2025) as representative methods. The

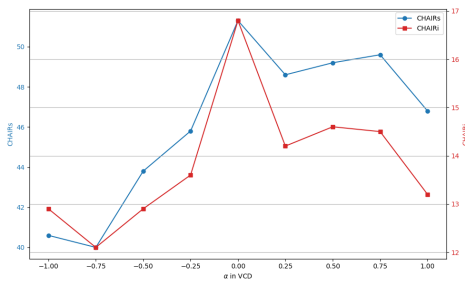
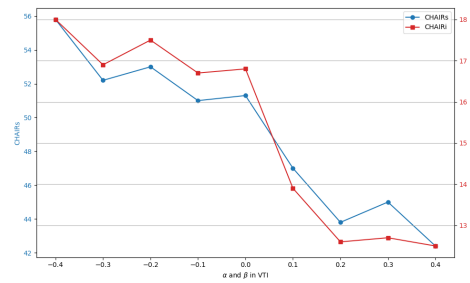
1026
1027
1028 Table 14: Evaluation on the generalization ability of HIRE
1029
1030
1031
1032

Model	$\text{CHAIR}_S \downarrow$	$\text{CHAIR}_I \downarrow$
LLaVA-1.5	51.3	16.8
+Ours (trained on VG_100K)	30.6	10.5
+Ours (trained on MSCOCO)	30.2	9.7

1033
1034 Table 15: Evaluation on the stability of HIRE
1035
1036
1037

	$\text{CHAIR}_S \downarrow$	$\text{CHAIR}_I \downarrow$
baseline	51.3	16.8
1	32.0	9.9
2	30.0	9.3
3	31.6	9.6
4	28.4	9.1
5	30.4	9.1
Average	30.5 ± 1.3	9.4 ± 0.31

1045 results are shown as Fig 7 and Fig 8. It can be observed that the CD-based method exhibits unstable
1046 performance in hallucination control. While VTI demonstrates a certain level of hallucination control
1047 capability, its performance exhibits significant fluctuations as the parameter varies. To quantify the
1048 effect of hallucination control, we employ coefficients of determination R^2 (Draper, 1998) as an
1049 evaluation metric. Our method demonstrate superior hallucination control capabilities, with R^2 scores
1050 of 0.97 on CHAIRs and 0.96 on CHAIRi, compared to VTI’s scores of 0.92 and 0.87, respectively.

1051
1052
1053
1054
1055
1056
1057
1058
1059
1060
1061 Figure 7: Control hallucination generation
1062 via the hyperparameter α in VCD (Leng et al.,
1063 2024).1064
1065
1066 E MORE QUALITATIVE ANALYSIS
1067
1068 To more explicitly demonstrate the effectiveness of our method in mitigating hallucinations in
1069 generative tasks, we visualize several examples, as illustrated in Fig. 9. For each image-prompt
1070 pair, we compare the responses generated by the original model and our method. Hallucinated
1071 words are highlighted in red, while newly identified objects that were missed by the original output
1072 are highlighted in blue to emphasize our method’s enhanced perceptual accuracy. As shown in
1073 Fig. 10, we further show the ability of controlling hallucination of HIRE. Additionally, as shown in
1074 Fig. 11, we present several examples from discriminative tasks to further validate the robustness and
1075 generalization capability of our approach across different settings.
1076
1077
1078
1079

1080

1081

1082

1083

1084

1085

1086

1087

1088

1089

1090

1091

1092

1093

1094

1095

1096

1097

1098

1099

1100

1101

1102

1103

1104

1105

1106

1107

1108

1109

1110

1111

1112

1113

1114

1115

1116

1117

1118

1119

1120

1121

1122

1123

1124

1125

1126

1127

1128

1129

1130

1131

1132

1133



LLaVA-1.5: The image features a large, well-lit bathroom with a white bathtub and a shower stall. The bathtub is situated next to a window, allowing natural light to fill the room. The shower stall is located on the left side of the bathroom. There are several bottles placed around the bathroom, with some near the bathtub and others on the right side of the room. **A toothbrush can be seen on the right side of the bathroom, and a cup is located near the center of the room.** The bathroom appears to be well-maintained and clean.

Ours: The image features a large, clean bathroom with a white bathtub and a window. The bathroom is well-lit, with natural light coming in through the window. The tub is situated next to a sink, and **there is a mirror above the sink.** The bathroom also has a shower area, which is likely to be a separate room. The overall atmosphere of the bathroom is bright and inviting.



Q: Please describe this image in detail.

LLaVA-1.5: The image features a large, ornate building with a clock tower at the top. The clock is prominently displayed on the tower, making it a focal point of the building. The building is situated in a city, surrounded by other buildings and a street. **There are several people in the scene, with some standing closer to the building and others further away. A car can be seen parked on the street, and a traffic light is visible in the background.** The overall atmosphere of the image suggests a bustling urban environment.

Ours: The image features a large building with a clock tower prominently displayed on its side. The clock tower is situated near the top of the building, and it appears to be the focal point of the scene. The building has a unique design, and it is situated in a city with a sky background. The scene is set against a backdrop of a cloudy sky, giving the impression of a sunny day.



Q: Please describe this image in detail.

LLaVA-1.5: The image features a white room with a large window that allows natural light to fill the space. A vase filled with flowers is placed **on a table near the window**, adding a touch of color and life to the room. **The room also has a doorway, which leads to another room.** In addition to the vase, **there is a potted plant in the room**, providing a sense of nature and greenery. The combination of the flowers, the potted plant, and the natural light from the window creates a pleasant and inviting atmosphere.

Ours: The image features a white room with a large window that allows natural light to fill the space. The room is decorated with a beautiful floral wallpaper, and a vase with flowers is placed **on the window sill.** The vase is filled with flowers, adding a touch of color and elegance to the room. The combination of the white walls, the floral wallpaper, and the vase with flowers creates a serene and inviting atmosphere.



Q: Please describe this image in detail.

LLaVA-1.5: The image features a giraffe standing in a fenced enclosure, surrounded by trees. The giraffe is positioned in the center of the scene, with its long neck and legs visible. The enclosure appears to be a part of a zoo, as **there are several other birds scattered throughout the area. Some birds are perched on the fence, while others are flying or walking around the enclosure.** The scene captures the giraffe's natural habitat and the presence of other animals in the same space.

Ours: The image features a giraffe standing in a fenced-in area, possibly in a zoo. The giraffe is positioned in the center of the scene, with its long neck and legs prominently visible. The fenced area is surrounded by trees, providing a natural and serene environment for the giraffe. The giraffe appears to be looking at the camera, possibly enjoying the attention it receives.



Q: Please describe this image in detail.

LLaVA-1.5: The image captures a group of people enjoying a day at the beach. There are four people in the scene, with two of them sitting on a blanket, and the other two standing nearby. They are all gathered around a surfboard, which is placed on the sand. The beach setting includes a chair positioned towards the left side of the image, and **a backpack can be seen placed on the sand.** The atmosphere appears to be relaxed and fun, as the group of friends spends time together on the beach.

Ours: The image depicts a group of people enjoying a day at the beach. There are four people in total, with two of them sitting on the sand, and the other two standing nearby. They are all wearing bathing suits and are relaxing on the beach. The beach scene also includes a surfboard, which is placed on the sand, and a chair, which is situated near the group of people. The overall atmosphere appears to be a fun and leisurely day spent at the beach.



Q: Please describe this image in detail.

LLaVA-1.5: The image captures a woman in a green shirt playing with a red frisbee in a grassy field. She is in the process of throwing the frisbee, which is positioned in the middle of the scene. There are several other people in the background, some of them closer to the woman and others further away. **A handbag can be seen placed on the ground near the left side of the scene.** The overall atmosphere of the image is lively and fun, as everyone seems to be enjoying their time outdoors.

Ours: The image captures a woman in a green shirt playing with a red frisbee in a park. She is in the middle of throwing the frisbee, which is visible in the air. The park is surrounded by trees, providing a pleasant and natural setting for the activity. There are several other people in the park, **some of whom are sitting on the grass, enjoying the outdoors.** The scene is lively and full of energy, as people engage in various activities and enjoy the pleasant weather.

Figure 9: Some examples of generative tasks on the COCO dataset, with hallucinated content highlighted in red and newly added correct content displayed in blue.

1134

1135

1136

1137

1138

1139

1140

1141

1142

1143

1144

1145

1146

1147


Q: Please describe this image in detail.

Original output: The image features a man wearing a white shirt and a red tie, standing in a room. He is making a hand gesture, **possibly giving the middle finger**, while looking at the camera. The man appears to be a waiter, as he is wearing a name tag. In the room, there is a **potted plant** located on the left side, and a **clock** can be seen hanging on the wall. The man is the main focus of the scene, and his hand gesture adds a sense of personality to the image.

Positive edit: The image features a man wearing a red tie and a white shirt, **standing in front of a mirror**. He is holding up his hand and **making a peace sign with his fingers**. The man appears to be enjoying himself and having a good time.

Negative edit: The image features a man wearing a white shirt and a red tie, standing in a room. He is **making the "I Love You" hand gesture**, with his fingers pointing upwards. The man is also wearing a name tag, which is visible on his shirt. In the room, there is a **potted plant** located on the left side, and a **clock** can be seen on the right side. A **chair** is also present in the scene, situated in the lower-left corner.


Q: Please describe this image in detail.

Original: The image captures a lively scene on a sidewalk where a young man is skillfully riding a skateboard. He is performing a trick, possibly a kickflip, as he moves down the sidewalk. There are several other people in the scene, some of whom are standing or walking nearby. A bench can be seen in the background, providing a place for people to sit and enjoy the atmosphere. Additionally, there are **a few bottles** scattered around the area, possibly belonging to the people present.

Positive edit: The image captures a young man skillfully riding a skateboard down a sidewalk. He is wearing a black jacket and appears to be enjoying his ride. There are several other people in the scene, some of whom are standing or walking nearby. The sidewalk is lined with benches, providing a comfortable space for people to sit and relax. The presence of multiple benches and people in the area suggests that this might be a popular spot for people to gather and socialize.

Negative edit: The image captures a man riding a skateboard down a sidewalk, with several people watching him perform the trick. The skateboarder is in the center of the scene, while the onlookers are scattered around him. There are a total of **11 people in the scene**, with some standing closer to the skateboarder and others further away. A bench can be seen in the background, and a **fire hydrant** is also visible in the scene. In addition to the skateboarder, there is a person **holding a cell phone**, possibly capturing the moment or communicating with someone.


Q: Please describe this image in detail.

Original output: The image features a stove top oven with a black stove top and a glass window. The oven is located in a kitchen, and it appears to be empty. The stove top is surrounded by a wooden countertop. In the kitchen, there are a few items scattered around. A **bottle** can be seen on the left side of the oven, and a **cup** is placed on the right side. Additionally, there is a **bowl** located near the center of the scene.

Positive edit: The image features a stove top oven with a metal surface, placed on a wooden counter. The oven has a clear glass door, allowing us to see the interior. The stove is equipped with a **set of knobs**, which are likely to control the temperature and cooking functions. The oven is situated in a kitchen setting, and the countertop is made of wood.

Negative edit: The image features a stove with a glass door, which is **open** and revealing a **blue and white towel**. The stove is situated on a wooden countertop. The stove is equipped with a burner and a cooktop, and it is surrounded by a variety of utensils and appliances. There are several **knives**, with one located near the top left corner, another in the middle, and a third on the right side. A **spoon** is also visible in the middle of the scene. A **cup** can be found on the left side of the stove, and a **bowl** is placed near the center. A **toaster** is present on the left side of the stove, and a **book** is located on the left side of the stove, possibly a cookbook or a recipe guide.


Q: Please describe this image in detail.

Original: The image showcases a beautiful cityscape with a large clock tower, Big Ben, towering over the city. The clock tower is situated in the middle of the scene, surrounded by other buildings. The city is bustling with activity, as numerous cars are scattered throughout the area, some closer to the foreground and others further in the background. In addition to the cars, there are **two trucks** visible in the scene, one near the center and the other towards the right side. The combination of the clock tower, the city's architecture, and the vehicles creates a lively and dynamic urban environment.

Positive edit: The image features a beautiful cityscape with a large clock tower prominently visible in the background. The clock tower is situated in the middle of the scene, surrounded by a variety of buildings. The cityscape is bustling with activity, as numerous cars are driving around the area, adding to the lively atmosphere. The scene also includes a **bridge**, which is a prominent feature in the background, and a **river** that runs through the city. The overall view of the cityscape is breathtaking, showcasing the city's architectural beauty and the dynamic nature of the urban environment.

Negative edit: The image showcases a bustling cityscape with a large clock tower, Big Ben, towering over the city. The clock is visible on the side of the tower, and the city is filled with various buildings, including a large castle. In the foreground, there is a busy street with cars and a **truck**, as well as a **bus**. A **person** can be seen walking on the sidewalk, and a **traffic light** is visible in the middle of the scene. The clock is positioned in the middle of the scene, and the cityscape is filled with buildings, creating a sense of depth and scale.

Figure 10: Some examples show that HIRE can amplify or mitigate hallucination by adjust the hyperparameter α .

1181

1182

1183

1184

1185

1186

1187

1188

1189

1190

1191

1192

1193

1194

1195

1196

1197

1198

1199

1200

1201

1202

1203

1204

1205

1206

1207

1208

1209

1210

1211

1212

1213

1214

1215

1216

1217

1218

1219

1220

1221

1222

1223

1224

1225

1226

1227

1228

1229

1230

1231

1232

1233

1234

1235

1236

1237

1238

1239

1240

1241

 <p>Q: Is there a cup in the image? Answer: No LLaVA-1.5: Yes Ours: No</p>	 <p>Q: Is there a car in the image? Answer: No LLaVA-1.5: Yes Ours: No</p>	 <p>Q: Is there a car in the image? Answer: Yes LLaVA-1.5: No Ours: Yes</p>	 <p>Q: Is there a pizza in the image? Answer: Yes LLaVA-1.5: No Ours: Yes</p>
 <p>Q: Is there a person in the image? Answer: No LLaVA-1.5: Yes Ours: No</p>	 <p>Q: Is there a dining table in the image? Answer: No LLaVA-1.5: Yes Ours: No</p>	 <p>Q: Is there a sports ball in the image? Answer: Yes LLaVA-1.5: No Ours: Yes</p>	 <p>Q: Is there a cup in the image? Answer: No LLaVA-1.5: Yes Ours: No</p>

Figure 11: Some examples of discriminative tasks on the COCO dataset.